Inertial active ratchet: Simulation versus theory

M. Muhsin and M. Sahoo ⓞ*

Department of Physics, University of Kerala, Kariavattom, Thiruvananthapuram-695581, India

We present the inertial active dynamics of an Ornstein-Uhlenbeck particle in a piecewise sawtooth ratchet potential. Using the Langevin simulation and matrix continued fraction method (MCFM), the particle transport, steady-state diffusion, and coherence in transport are investigated in different parameter regimes of the model. Spatial asymmetry is found to be a key criterion for the possibility of directed transport in the ratchet. The MCFM results for net particle current of overdamped dynamics of the particle agree well with the simulation results. The simulated particle trajectories for the inertial dynamics and the corresponding position and velocity distribution functions reveal that the system passes through an activity-induced transition in the transport from the running phase to the locked phase of the dynamics. This is further corroborated by the mean square displacement (MSD) calculations, where the MSD gets suppressed with increase in the persistent duration of activity or self-propulsion in the medium and finally approaches zero for a very large value of self propulsion time. The nonmonotonic behavior of the particle current and Péclet number with self-propulsion time confirms that the particle transport and its coherence can be enhanced or reduced by fine tuning the persistent duration of activity. Moreover, for intermediate ranges of self-propulsion time as well as mass of the particle, even though the particle current shows a pronounced unusual maximum with mass, there is no enhancement in the Péclet number, instead the Péclet number decreases with mass, confirming the degradation of coherence in transport.

I. INTRODUCTION

Noise is omnipresent and is an indispensable part of nature, which plays an important role in the dynamics of systems operating at microscopic length scale [1,2]. A system that generates an unidirectional transport out of a noisy environment utilizing nonequilibrium condition and spatial (or temporal) asymmetry is referred as a Brownian ratchet [3–5]. However, in recent days, there is an immense interest in active ratchets, which is a growing area of research because of its enormous applications in the fabrication of different types of nanorobots, artificial swimmers, and other self-driven systems [6]. Active ratchets are understood through the use of active matter systems consisting of self propelled units [7–13]. Such self-propelled units are known as active particles, and they have the ability to self-propel on their own by consuming energy from the environment. Hence, they are inherently driven away from equilibrium, and the nonequilibrium condition is the intrinsic property of such systems [6,14,15]. Examples of such systems range from the microscopic to macroscopic length scale such as unicellular organisms like motile bacteria [16,17], self-motile Janus particles [18,19], micro and nanorobots [20,21], hexbugs [22], flocking of birds [23], school of fishes [24], etc. The most commonly used models for studying the dynamical behavior in such active systems are active Brownian particle (ABP) model [25–28], active Ornstein-Uhlenbeck particle(AOUP) model [29–31], and run-and-tumble particle model [32,33].

Unidirectional transport in active ratchets are experimentally realized even in the absence of an external bias unlike passive Brownian ratchets [7,10,11]. When self-propelled particles are placed in an asymmetric potential, the particles on an average can travel to the gentler side of the potential giving rise to unidirectional transport with a nonzero net particle flux [10,11,13]. The rectification effect of active matter in a periodic structure was first observed for run-and-tumble bacteria moving through funnel-shaped barriers [9]. Thereafter, the rectification effect in active matter is studied using both theoretical and numerical approaches for different types of systems [8,10,11,34–49]. To name a few, from the simulation results of the dynamics of active Janus particles in an asymmetric channel, it is confirmed that the rectification can be orders of magnitude stronger than that of ordinary thermal ratchets [35]. Similarly, in Ref. [36], it is reported that the spatially modulated self-propelled velocity can also induce directed transport [36]. The emergence of the active ratcheting effect for run-and-tumble particles in an asymmetric piecewise periodic potential is reported in Ref. [8]. Rectification of twitching bacteria through two dimensional (2D) narrow channel is investigated numerically using both tug-of-war model and run-and-tumble model [37]. The phenomena of current reversal is observed for inertial active dynamics of particles (using the ABP model) in a sawtooth ratchet potential for certain regimes of parameter space [38–40]. In most of these studies, the rectification effect in asymmetric periodic structures is found to be a general feature of active matter [36,41–49].

Despite such rigorous works on active ratchets using different models, the study of rectification effect especially
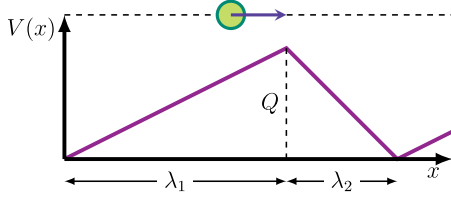
---

*jolly.iopb@gmail.com

FIG. 1. Schematic of the ratchet potential [Eq. (4)].

employing AOUP model is only reported in a few literature. For instance, the underdamped dynamics of a Brownian particle driven by Ornstein-Uhlenbeck (OU) noise in a periodic asymmetric potential is studied in Ref. [50] using both Langevin simulation and analytical approaches, such as generalized unified colored noise approximation method (UCNA), path integral approach, and numerical matrix continued fraction method (MCF) methods. Their main finding is the current reversal with variation of noise correlation time as well as mass of the particle. Similarly, the overdamped dynamics of a particle in a correlation ratchet, driven by both additive Gaussian white and OU noise is studied both numerically using the MCF method and analytically using the UCNA method in Ref. [51]. Here, the authors have also observed the current reversal phenomena at a particular range of noise color, but for an appropriately chosen shape of the ratchet potential.

In this paper, using both Langevin simulation and the MCF method, we examine the transport behavior of an inertial active OU particle in a piecewise sawtooth ratchet potential, which is largely unexplored. We simulate both underdamped and overdamped dynamics of the particle and obtain the particle trajectory, steady-state distribution functions, particle current, diffusion coefficient, and Péclet number as a function of parameters of the model. The obtained average current of the overdamped dynamics of the particle using MCF method is in good agreement with the simulation result. Furthermore, it matches with the simulated underdamped particle current in highly viscous regime as expected. The system is found to pass through an activity controlled transition in transport from the running phase to the locked phase of the dynamics. The transport properties and coherence in transport are investigated in various parameter regimes. Moreover, the current reversal phenomena is not observed in any of the parameter regimes of the model, unlike Refs. [50,51].

II. MODEL AND METHOD

We consider the motion of an inertial active Ornstein-Uhlenbeck particle of mass m through a ratchet potential. The dynamics of the particle is given by the Langevin's equation of motion [28,50,52–54],

$$m\ddot{x} = -\gamma\dot{x} - V'(x) + \xi(t), \tag{1}$$

with x being the position coordinate and $v = \dot{x}$ as the velocity coordinate of the particle. Here, γ is the viscous coefficient of the medium, and $V(x)$ is the confining ratchet potential, which is periodic in nature with periodicity λ. $\xi(t)$ is the exponentially correlated noise with strength C, which follows

the Ornstein-Uhlenbeck process [30] as

$$t_c\dot{\xi}(t) = -\xi(t) + \sqrt{2C}\,\eta(t). \tag{2}$$

Here, $\eta(t)$ is the δ correlated Gaussian white noise, which satisfies the properties $\langle\eta(t)\rangle = 0$ and $\langle\eta(t)\eta(s)\rangle = \delta(t-s)$. We set C to be unity throughout our paper. The angular bracket $\langle\cdots\rangle$ denotes the ensemble average over noise. The statistical properties of the Ornstein-Uhlenbeck noise $\xi(t)$ is given by

$$\langle\xi(t)\rangle = 0, \quad \langle\xi(t)\xi(s)\rangle = \frac{C}{t_c}\exp\left(-\frac{|t-s|}{t_c}\right), \tag{3}$$

where t_c represents the noise correlation time. It is the time up to which the particle self-propels in the ratchet and, hence, activity persists in the medium for a time interval of t_c. A finite t_c notably quantifies the presence of activity or correlation in the medium, that decays exponentially with t_c. For a nonzero t_c value, the system is inherently driven away from equilibrium [55]. However, in the passive limit ($t_c \to 0$ limit) of our model, we consider the strength of noise C to be $\gamma k_B T$ (fluctuation-dissipation relation) in order for the system to approach the typical thermal equilibrium limit of the dynamics at temperature T [56,57]. The potential $V(x)$ that appears in Eq. (1) has the form

$$V(x) = \begin{cases} \frac{Q}{\lambda_1}x, & x \leqslant \lambda_1, \\ \frac{Q}{\lambda_2}(\lambda - x), & \lambda_1 < x \leqslant \lambda. \end{cases} \tag{4}$$

Here, Q is the potential height and $\lambda = \lambda_1 + \lambda_2$ is the periodicity of the ratchet potential (see Fig. 1). Equation (4) represents a sawtooth potential which is symmetric when $\lambda_1 = \lambda_2$. Therefore, we introduce an asymmetric parameter Δ such that $\Delta = \lambda_1 - \lambda_2$.

In this paper, we are mainly interested in the particle transport, associated dispersive spread or diffusion, and coherence in transport of the particle. The particle transport can be quantified by measuring an essential quantity, known as particle current. As per the geometry of the ratchet potential, the motion of the particle is along the x direction and, hence, the average particle current in the stationary state can be defined as [3,58]

$$\langle j \rangle = \lim_{t\to\infty}\left\langle\frac{x(t) - x(0)}{t}\right\rangle. \tag{5}$$

Similarly, the diffusive spread or diffusion can be quantified by measuring the diffusion coefficient D about the mean position of particle, which is given by [59]

$$D = \lim_{t\to\infty}\frac{\langle x^2 \rangle - \langle x \rangle^2}{2t}. \tag{6}$$

Here, $\langle x^2 \rangle - \langle x \rangle^2$ represents the mean square displacement (MSD) of the particle. The transport of the particle in such an asymmetric potential and stochastic environment depends on the diffusive spread and the mean velocity of the particle. The effectiveness or coherence in the transport can be quantified by measuring a dimensionless parameter called Péclet number Pe, which is defined as

$$\text{Pe} = \frac{\langle j \rangle\lambda}{D}. \tag{7}$$

We have set the periodicity of the potential λ as unity throughout this paper.

III. RESULTS AND DISCUSSION

The Fokker-Planck equation corresponding to the dynamics in Eq. (1) for the probability density function $P(x, v, \xi; t)$ is given by

$$
\frac{\partial P}{\partial t} = -v \frac{\partial P}{\partial x} + \frac{\partial}{\partial v} \left(\frac{\gamma v}{m} + \frac{V'(x)}{m} - \frac{\xi(t)}{m} \right) P
$$
$$
+ \frac{\partial}{\partial \xi} \left(\frac{\xi}{t_c} + \frac{C}{t_c^2} \frac{\partial}{\partial \xi} \right) P. \tag{8}
$$

It is not possible to obtain the exact analytical solution of Eq. (8) even for the steady-state because of the nonlinearity in the gradient of the potential function $V(x)$. However, the steady-state solution is possible for $P(x, v, \xi; t)$ with the help of numerical approximation schemes. In order to investigate the transport of the particle, one can solve the dynamics either by directly simulating Eq. (1) or by employing the MCF method to Eq. (8) for the approximate steady-state solution of $P(x, v, \xi)$.

For the overdamped dynamics of the particle, the inertial term in Eq. (1) is neglected, and the corresponding probability density function $P(x, \xi; t)$ satisfies the Fokker-Planck equation [51,60],

$$
\frac{\partial P}{\partial t} = \frac{\partial}{\partial x} \left(\frac{V'(x)}{\gamma} - \frac{\xi}{\gamma} \right) P + \frac{\partial}{\partial \xi} \left(\frac{\xi}{t_c} + \frac{C}{t_c} \frac{\partial}{\partial \xi} \right) P. \tag{9}
$$

In the stationary state or steady-state limit, the probability density function $P(x, \xi; t)$ satisfies

$$
\frac{\partial P}{\partial t} = 0. \tag{10}
$$

In order to find the approximate solution of Eq. (10) for the stationary state probability distribution function $P(x, \xi)$, it can be expanded in complete sets of functions in both variables x and ξ using a set of Hermite functions. Since the potential is periodic in nature, $P(x, \xi)$ can take the form [51]

$$
P(x, \xi) = \phi_0(\xi) \sum_{p=0}^{\infty} \sum_{\mu=-\infty}^{\infty} c_p^\mu e^{2\pi i \mu x / \lambda} \phi_p(\xi). \tag{11}
$$

Here, the prefactor $\phi_0(\xi)$ is introduced for the simplification of mathematical calculations and $\phi_p(\xi)$ is the set of Hermite functions given by

$$
\phi_p(\xi) = \frac{1}{\sqrt{\alpha 2^p p! \sqrt{\pi}}} e^{\left(\frac{-\xi^2}{2\alpha^2} \right)} H_p \left(\frac{\xi}{\alpha} \right), \tag{12}
$$

with α as the scaling parameter considered as $\alpha = \sqrt{\frac{2D}{t_c}}$ and $H_p(x)$ is the Hermite polynomial. For $p = 0$, Eq. (12) yields $\phi_0(\xi)$ as

$$
\phi_0(\xi) = \frac{1}{\sqrt{\alpha \sqrt{\pi}}} e^{\left(\frac{-\xi^2}{2\alpha^2} \right)}. \tag{13}
$$

Since the potential $V(x)$ is periodic in nature, the force exerted by the potential, $f(x) = -V'(x)$ can be expanded in terms of Fourier series as

$$
f(x) = \sum_{l=-\infty}^{\infty} f_l e^{2\pi i l x / \lambda}. \tag{14}
$$

Substituting Eq. (11) in Eq. (10) and using Eqs. (12) and (14), we obtain a tridiagonal vector recurrence relation in terms of expansion coefficients c_p^μ as

$$
Q_p^- c_{p-1} + Q_p c_p + Q_p^+ c_{p+1} = 0, \tag{15}
$$

with

$$
Q_p^- = \sqrt{\frac{pC}{t_c}} B, \tag{16}
$$

$$
Q_p = A - \frac{p}{t_c} I, \tag{17}
$$

and

$$
Q_p^+ = \sqrt{\frac{(p+1)C}{t_c}} B. \tag{18}
$$

Here, c_p is a column matrix consisting of the elements c_p^0, c_p^1, and $c_p^2 \cdots c_p^\mu$. The elements of matrices A and B are given by

$$
[A_{n,m}] = \frac{2\pi i n}{\gamma \lambda} f_{n-m}, \tag{19}
$$

$$
[B_{n,m}] = -\frac{2\pi i m}{\gamma \lambda} \delta_{n,m}, \tag{20}
$$

with I being the identity matrix. The vector recurrence relation in Eq. (15) can be solved numerically using the MCF method as described in Ref. [60]. For this purpose, we introduce the matrix S_p such that

$$
c_{p+1} = S_p c_p. \tag{21}
$$

Now, substituting Eq. (21) in Eq. (15), we obtain

$$
Q_p^- c_{p-1} + (Q_p + Q_p^+ S_p) c_p = 0. \tag{22}
$$

Further solving Eq. (22), we obtain the matrix S_p as the matrix continued fraction,

$$
S_p = -(Q_{p+1} + Q_{p+1}^+ S_{p+1})^{-1} Q_{p+1}^-. \tag{23}
$$

For $p = 0$, Eq. (22) takes the form

$$
(Q_0 + Q_0^+ S_0) c_0 = 0. \tag{24}
$$

Normalization of the steady-state probability distribution $P(x, \xi)$,

$$
\int_0^\lambda dx \int_{-\infty}^\infty d\xi \, P(x, \xi) = 1, \tag{25}
$$

yields

$$
c_0^0 = \frac{1}{\lambda}. \tag{26}
$$

Using this arbitrary component c_0^0 in Eqs. (24) and (21), we have numerically evaluated all the components of c_p. In order to find the average particle current, the Fokker-Planck

equation [Eq. (9)] can be written in the form of a continuity equation as

$$\frac{\partial P(x,\xi;t)}{\partial t} = -\frac{\partial \rho_x(x,\xi;t)}{\partial x} - \frac{\partial \rho_\xi(x,\xi;t)}{\partial \xi},\qquad(27)$$

where $\rho_x(x,\xi;t)$ and $\rho_\xi(x,\xi;t)$ are the probability currents in the x and ξ directions, respectively. Next, comparing Eq. (27) with Eq. (9), we get

$$\rho_x(x,\xi;t) = \left(\frac{f(x)}{\gamma} - \frac{\xi}{\gamma}\right)P(x,\xi;t).\qquad(28)$$

Hence, the average stationary current in the x direction over a period can be calculated as

$$\langle j \rangle = \frac{1}{\lambda}\int_0^\lambda dx \int_{-\infty}^\infty d\xi\, \rho_x^{(st)}(x,\xi)$$

$$= \frac{1}{\gamma}\left[-\sum_{\mu=-\infty}^\infty f_\mu c_0^{-\mu} + \frac{C}{t_c}c_1^0\right].\qquad(29)$$

Now, substituting the components $c_0^{-\mu}$ and c_1^0 of the column matrix c_p, we have numerically evaluated the average particle current $\langle j \rangle$.

Proceeding in the same way as for the overdamped case described above, one can solve Eq. (8) for the steady-state probability distribution $P(x,v;\xi)$ of the underdamped dynamics of the particle and find out the average particle current. The approximate steady-state solution of Eq. (8) can take the form

$$P(x,v,\xi)$$

$$= \phi_0(\xi)\psi_0(v)\sum_{r=0}^\infty\sum_{p=0}^\infty\sum_{\mu=-\infty}^\infty c_{p,r}^\mu e^{2\pi i\mu x/\lambda}\phi_p(\xi)\psi_r(v).$$

$$(30)$$

Here, $\psi_r(v)$ is the Hermite function given by

$$\psi_r(v) = \frac{1}{\sqrt{\beta 2^r r!}\sqrt{\pi}}e^{\left(\frac{-v^2}{2\beta^2}\right)}H_r\left(\frac{v}{\beta}\right),\qquad(31)$$

with β being a scaling parameter. Following the same method discussed earlier, we get the recursion relation in terms of $c_{p,r}^\mu$,

$$A_{p,r}c_{p,r-2} + B_{p,r}c_{p,r-1} + \Gamma_{p,r}\,c_{p,r} + E_{p,r}c_{p,r+1}$$
$$+Z_{p,r}c_{p-1,r-1} + \Theta_{p,r}c_{p+1,r-1} = 0.\qquad(32)$$

Here, A, B, Γ, E, Z, and Θ are matrices whose elements are given by

$$[A_{\mu,\nu}]_{p,r} = -\frac{\gamma}{m}\sqrt{(r-1)r}\,\delta_{\mu,\nu},$$

$$[B_{\mu,\nu}]_{p,r} = \frac{\sqrt{2r}}{\beta m}f_{\mu-\nu} - \frac{i\nu k\beta\sqrt{r}}{\sqrt{2}}\,\delta_{\mu,\nu},$$

$$[\Gamma_{\mu,\nu}]_{p,r} = -\left(\frac{\gamma r}{m} + \frac{p}{t_c}\right)\delta_{\mu,\nu},$$

$$[E_{\mu,\nu}]_{p,r} = -\frac{i\nu k\beta\sqrt{r+1}}{\sqrt{2}}\,\delta_{\mu,\nu},$$

$$[Z_{\mu,\nu}]_{p,r} = \frac{\alpha\sqrt{rp}}{m\beta}\,\delta_{\mu,\nu},$$

and

$$[\Theta_{\mu,\nu}]_{p,r} = \frac{\alpha}{m\beta}\sqrt{r(p+1)}\,\delta_{\mu,\nu},$$

respectively. $c_{p,r}$ is a column matrix given as

$$c_{p,r} = \left[\cdots c_{p,r}^{-1}c_{p,r}^0 c_{p,r}^1 \cdots\right]^T.$$

By numerically solving Eq. (32) and using the column matrix $c_{p,r}$, one can compute the steady-state probability distribution and the average current.

We have also simulated the dynamics [Eq. (1)] using Heun's method algorithm. Since we have considered an one-dimensional ratchet potential, the transport of the particle is along the x direction of the potential $V(x)$. The periodic boundary condition is imposed along the x axis with periodicity of the potential $V(x+\lambda) = V(x)$. The physical quantities of interest are evaluated by integrating the equation of motion [Eq. (1)] using a second order modified Euler's scheme (Heun's method). The Ornstein-Uhlenbeck noise $\xi(t)$ is implemented in the dynamics using the Fox method approach as described in Ref. [61]. An integral time step of 10^{-3} is considered in the simulation, and the total integration is taken over 10^5 time steps. The initial transients of 10^4 time steps are ignored in order for the system to attain steady state. The average values are obtained over 10^4 realizations.

The simulation results of particle trajectories, position, and velocity distribution functions of the particle for different values of t_c are shown in Fig. 2. For a very small value of t_c, the particle is merely influenced by the presence of potential barriers and distributed uniformly throughout the potential as shown in the position distribution plot of Fig. 2(d). The velocity distribution is Gaussian [see Fig. 2(a)] since the $t_c \to 0$ limit is the white noise limit. The trajectory of the particle [see Fig. 2(g)] does not show any signature of the presence of potential trap as expected. In the steady state, the magnitude of the noise correlation of the OU process [Eq. (3)] varies inversely with t_c such that $\langle \xi^2(t) \rangle = \frac{C}{t_c}$. Hence, for a very small value of t_c, even though the noise correlation persists for a very small interval of time, the intensity of the correlation is very high. As a result, the magnitude of random kicks on the particle is very large. Due to this, the particle does not feel the presence of the potential barrier and moves freely in both forward and backward directions of the ratchet potential, resulting an uniform distribution of the particles in the $t_c \to 0$ limit. This is expected as in the $t_c \to 0$ limit, the OU noise becomes white noise. In this limit, the system behaves as if it is in the running state.

With a further increase in t_c, the magnitude of the noise correlation decreases, and at the same time the duration of its persistence increases. The particle starts getting more and more confined at the potential minima and feels the influence of the barriers in both forward and backward directions of the ratchet potential. This is very well reflected from the position distribution of the particle in Fig. 2(e) with maximum probability of finding the particle in one of the potential minima. Due to the presence of asymmetry in the potential, the particle on an average makes more jumps towards the forward direction as compared to the backward direction of the potential. This can also be seen from the trajectory plotted in Fig. 2(h) where there are sudden jumps and stable regions
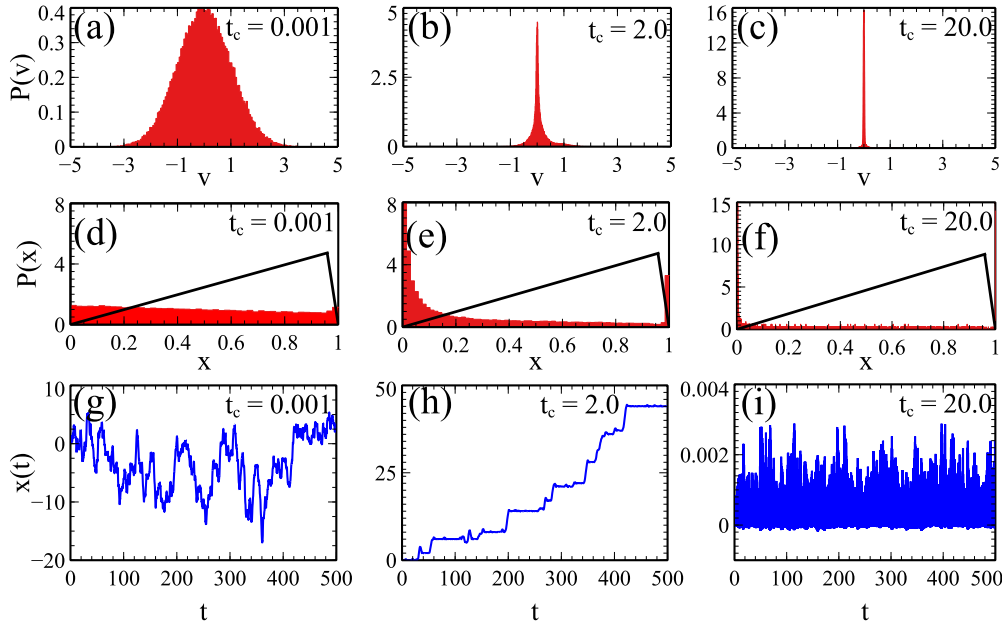
FIG. 2. (a)–(c) Velocity distribution $P(v)$ as a function of v for different values of t_c. (d)–(f) Position distribution $P(x)$ as a function of x for different values of t_c. The black solid line represents the corresponding sawtooth potential. (g)–(i) Particle trajectories are plotted for different values of t_c. The common parameters taken are $m = 1.0$, $\Delta = 0.9$, $Q = 0.5$, $C = 1$, and $\gamma = 1.0$.

indicating the presence of potential being felt by the particle. As a result, the velocity distribution becomes non-Gaussian with exponential tails in both the directions [see Fig. 2(b)]. In this regime, the value of $\langle \xi^2(t) \rangle$ is such that the particle becomes capable of overcoming the potential barrier in the direction with gentler slope of the potential. Hence, on average, a nonzero particle current is expected. For a very large t_c, the magnitude of the noise correlation [Eq. (3)] becomes very small, and the correlation persists for longer interval of time. Hence, the magnitude of the random kicks are very small and are not strong enough to make the particle escape from the potential minimum [see Figs. 2(f) and 2(i)]. This is the reason for which the velocity distribution approaches a δ function centered at zero [Fig. 2(c)] for a very large t_c value. In this limit, the system behaves as if it is trapped or in the locked state. Thus, with t_c, the system passes through a transition from the running state to the locked state of the particle transport.

Next, we have simulated the steady-state particle current $\langle j \rangle$ and diffusion coefficient D for different values of Δ, t_c, and Q. The 2D plots of $\langle j \rangle$ and D as a function of Δ and t_c are shown in Figs. 3(a) and 3(c), respectively. Similarly, we have shown the 2D plots of $\langle j \rangle$ and D as a function of Δ and Q in Figs. 3(b) and 3(d), respectively. From these plots, it is observed that for a given spatial asymmetry in the potential, $\langle j \rangle$ shows a nonmonotonic behavior with both t_c and Q values. Furthermore, the maximum current is found to be sensitive to the spatial asymmetry of the potential, and it increases with increase in the asymmetry parameter Δ whereas, diffusion shows decreasing behavior with both t_c and Q.

The plots of $\langle j \rangle$, D, and Pe as a function t_c are presented in Figs. 4(a)–4(c), respectively for different values of m. For a given mass of the particle, $\langle j \rangle$ shows a nonmonotonic behavior with t_c. It starts from zero and increases with t_c, attains the

maximum value for an intermediate range of t_c, and finally approaches back to zero value for larger t_c. With an increase in m, the critical value of t_c at which the current starts to flow, shifts towards the right. This suggests that for larger m, higher t_c is required to have a net current in the ratchet. At the same time, the maximum current gets suppressed with an increase in m and shifts towards the larger t_c value. This implies that for larger mass, the noise correlation in the dynamics has to persist for longer interval of time to obtain maximum current. On the other hand, D shows a decaying behavior with t_c as
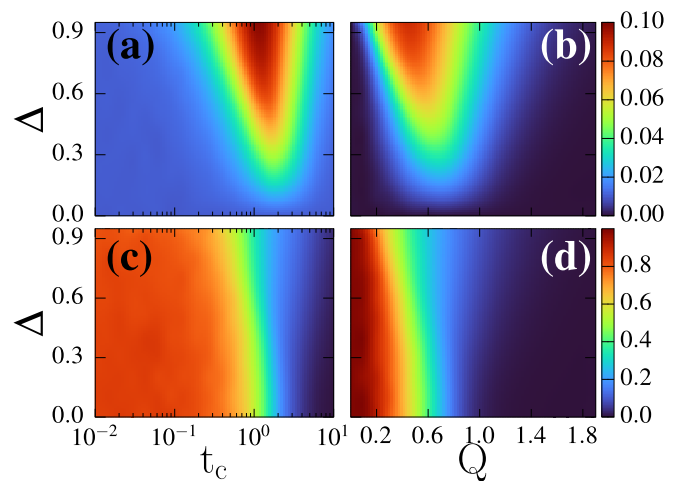

FIG. 3. (a) Two-dimensional plot of $\langle j \rangle$ as a function of Δ and t_c. (b) Two-dimensional plot of $\langle j \rangle$ as a function of Δ and Q. (c) Two-dimensional plot of D as a function of Δ and t_c. (d) Two-dimensional plot of D as a function of Δ and Q. The common parameters in (a) and (c) are $m = 1$, $C = 1$, $Q = 0.5$, and $\gamma = 1$ and in (b) and (d) are $m = 1$, $C = 1$, $t_c = 1$, and $\gamma = 1$.
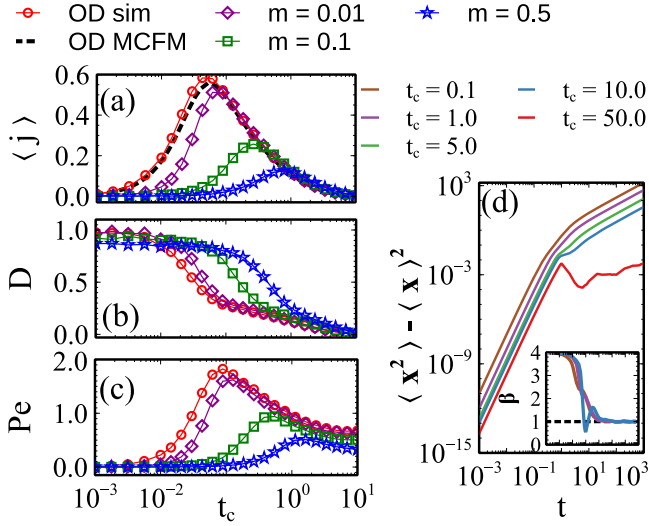
FIG. 4. $\langle j \rangle$, D, and Pe as a function of t_c for different values of m are shown in (a)–(c), respectively. The simulation results (OD sim) for $\langle j \rangle$, D, and Pe and the MCFM calculation results only for $\langle j \rangle$ (OD MCFM) are also plotted as a function of t_c for the overdamped case. MSD versus t is shown in (d) for different values of t_c and for $m = 0.5$. The inset of (d) shows the exponent β versus t. The other common parameters are $\gamma = 1$, $\Delta = 0.9$, $C = 1$, and $Q = 0.5$.

FIG. 5. Two-dimensional plots of (a) $\langle j \rangle$ and (b) D as a function of t_c and m. The other common parameters are: $\gamma = 1$, $\Delta = 0.9$, $C = 1$, and $Q = 0.5$.

in Fig. 4(b). For very small value of t_c, D has maximum value which persists as long as there is no net current in the ratchet. At the critical t_c, at which the current starts to flow, D also decays before approaching zero as expected. It is seen that the t_c at which the current has the maximum value, the diffusion shows a minima type feature as anticipated. Furthermore, diffusion in the lower t_c limit gets suppressed with mass of the particle. As the effectiveness of the transport can be understood by analyzing the behavior of the Péclet number, we have presented Pe with t_c in Fig. 4(c). Pe follows the same behavior as that of $\langle j \rangle$, confirming a coherent or reliable transport in the intermediate range of t_c.

In order to further understand the diffusive behavior of the transport, we have calculated the MSD, $\langle x^2 \rangle - \langle x \rangle^2$ and plotted as a function of t in Fig. 4(d) for different values of t_c. For a particular t_c, in the lower time regime, MSD is found to be proportional to t^4, hence, the transport is superdiffusive. On the other hand, in the long time regime, the transport is diffusive in nature as the MSD is proportional to t. With an increase in t_c, the MSD gets suppressed and approaches zero for very large t_c values, reflecting the trapping of the particle for longer persistence of noise correlation in the dynamics. To have a better clarity of the dependence of MSD with time, we introduce a parameter β such that MSD $\propto t^\beta$. The variation of β with time is shown in the inset of Fig. 4(d). In the lower time regime, β is found to be 4, which confirms the superdiffusive transport of the particle at short timescale. In the long time limit, β is one, which reflects the as usual steady-state diffusive behavior of the particle. On the other hand, $\langle x^2 \rangle$ shows different features. In the lower time limit, it is ballistic, i.e., $\langle x^2 \rangle \propto t^2$, irrespective of the persistence duration of noise correlation in the dynamics. In the long time limit or at the stationary state, $\langle x^2 \rangle$ depends on the correlation
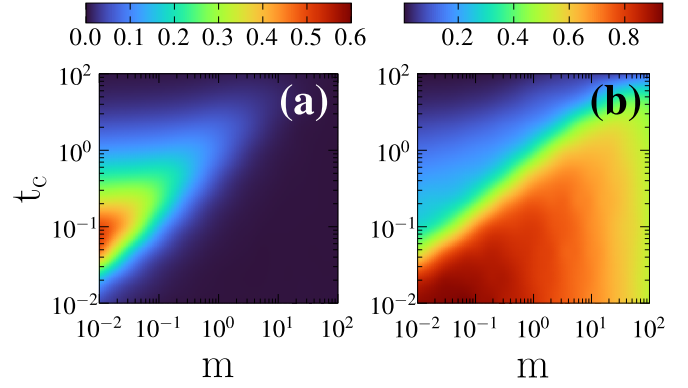
time. In this state, $\langle x^2 \rangle$ is diffusive (i.e., $\langle x^2 \rangle \propto t$) for the lower t_c limit, ballistic (i.e., $\langle x^2 \rangle \propto t^2$) for the intermediate t_c limit, and nondiffusive (i.e., independent of t) for the larger t_c limit. The different behavior of $\langle x^2 \rangle$ and MSD in the steady state are due to the nonzero value of $\langle x \rangle$ as it is proportional to time.

In Figs. 5(a) and 5(b), we depict the 2D plots of $\langle j \rangle$ and D, respectively, as a function of t_c and m. In the low t_c limit, the current shows a monotonically decreasing behavior whereas in the intermediate regime of t_c, it shows a nonmonotonic behavior with m. Similarly, the diffusion coefficient shows a decreasing behavior in the low t_c regime and increasing behavior in the intermediate t_c regime with m. In order to understand this unusual behavior of $\langle j \rangle$ with m in the intermediate range of t_c, we have plotted $\langle j \rangle$, D, and Pe vs m in Fig. 6 for different values of Δ and at two different t_c values. It is observed that the current increases with m and reaches a maximum value in the intermediate range of m, and this maximum value increases with the increase in asymmetry of the potential. With
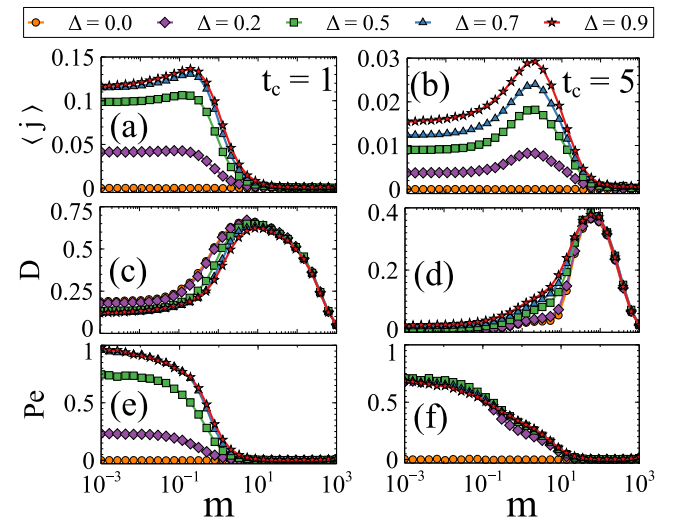

FIG. 6. $\langle j \rangle$, D, and Pe as a function of m with $t_c = 1$ for different values of Δ in (a), (c), and (e) and for $t_c = 5$ in (b), (d), and (f), respectively. The other common parameters are $\gamma = 1$, $Q = 0.5$, and $C = 1$.
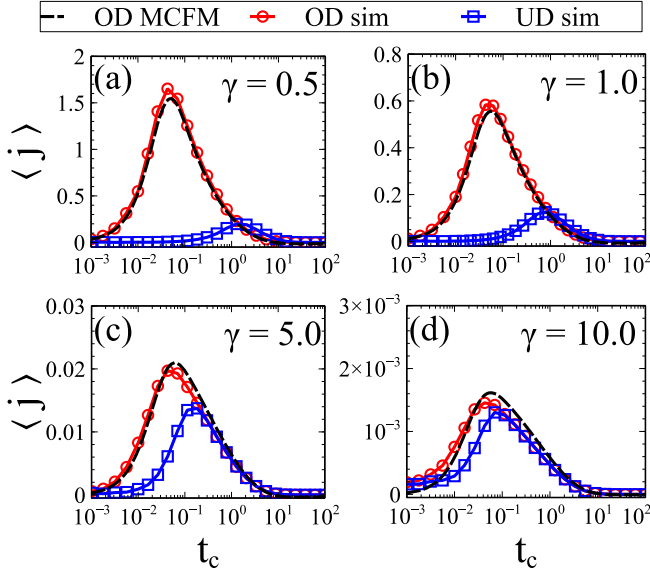
FIG. 7. The simulation results of $\langle j \rangle$ versus t_c both for overdamped (OD sim) and underdamped (UD sim) (with $m = 0.5$) cases along with the MCFM calculation (OD MCFM) for the overdamped case are presented in (a)–(d) for different values of γ. The other common parameters are $\Delta = 0.9$, $C = 1$, and $Q = 0.5$.

a further increase in the t_c value, even though the magnitude of current decreases, it shows a pronounced maximum as a function of m [see Fig. 6(b)]. D shows roughly a minimum exactly around the same point where the current shows a maximum. It starts increasing as a function of m from the point where current starts decreasing and finally shows a maximum at which the current approaches zero as expected. Although $\langle j \rangle$ as a function of m shows a well defined maximum, Pe does not follow the same behavior, rather it decreases with the increase in m. This reflects the degradation of the coherence in the particle transport.

Finally, the simulation results of $\langle j \rangle$ as a function of t_c for both overdamped dynamics (excluding the inertia term) and underdamped dynamics (with inertia) for different values of γ are presented in Fig. 7. The MCF method calculation results for the overdamped dynamics of the particle are also plotted for a comparison. The overdamped current is always larger than that of the underdamped current as expected. For all values of γ, the MCF method results for $\langle j \rangle$ of overdamped dynamics of the particle are in good agreement with the simulation results. Furthermore, the MCF method results of overdamped case approach the simulation results for $\langle j \rangle$ of underdamped case only for very large value of γ as anticipated. Most importantly, we do not see current reversal in any of the parameter regimes of either overdamped or underdamped dynamics of our model unlike inertial dynamics of active noninteracting particles in the sawtooth ratchet potential [38].

IV. SUMMARY

To summarize, we have studied the inertial active dynamics of an Orntsein-Uhlenbeck particle in a piecewise sawtooth ratchet potential. In particular, we have investigated the particle transport and coherence in transport with parameters of the model using both the MCF method and the Langevin simulations. The main findings of our paper are as follows. The analytical results for the average particle current of overdamped dynamics of the particle using the MCF method agree well with the simulation results. The MCF method results of average current of overdamped dynamics of the particle approaches the simulated particle current of inertial dynamics only when γ becomes very large as expected. It is observed that the system exhibits a transition in transport from running phase to the locked phase, that is controlled by the duration of self-propulsion of the particle or persistent duration of activity in the medium. The nature of particle current and Péclet number are found to be nonmonotonic with the self-propulsion time. They first increase, manifest a maximum, then decrease as the self-propulsion time increases and approach zero value for very large value of self-propulsion time. These observations suggest that the net particle transport and the coherence in transport can be controlled (enhanced or reduced) by fine tuning the persistent duration of activity in the medium. Moreover, the behavior of current also implies the entry of the particle from running phase to the locked phase of transport.

Furthermore, for an intermediate range of persistence of activity, the particle current shows a maximum as a function of mass of the particle, which is quite unusual and the absolute value of this maximum is quite sensitive to the potential asymmetry. Surprisingly, it is observed that even though the particle current increases with mass in certain regime of the parameter space, the Péclet number does not follow the same trend. Instead it decreases with increase in mass of the particle, confirming the degradation of reliability or coherence of transport. Moreover, we do not see the phenomena of current reversal in any of the parameter regimes of our model unlike Refs. [7,38,39]. We believe that the results obtained in our model can be experimentally realized in some active matter systems in the regime of the high Reynolds number. Also, we anticipate that our results for inertial active dynamics can provide a scheme for novel rectification device of active matter systems. It would be further interesting to extend this model for investigating the collective behavior and making use of the rectified motion in terms of stochastic energetic parameters.

[1] A. Einstein, Zur theorie der brownschen bewegung, Ann. Phys. (NY) **324**, 371 (1906).

[2] D. S. Lemons and A. Gythiel, Paul Langevin's 1908 paper "On the Theory of Brownian Motion" ["Sur la théorie du mouvement brownien," C. R. Acad. Sci. (Paris) **146**, 530 (1908)], Am. J. Phys. **65**, 1079 (1997).

[3] P. Reimann, Brownian motors: Noisy transport far from equilibrium, Phys. Rep. **361**, 57 (2002).

[4] R. D. Astumian, Thermodynamics and kinetics of a brownian motor, Science **276**, 917 (1997).

[5] M. O. Magnasco, Forced Thermal Ratchets, Phys. Rev. Lett. **71**, 1477 (1993).

[6] C. Bechinger, R. Di Leonardo, H. Löwen, C. Reichhardt, G. Volpe, and G. Volpe, Active particles in complex and crowded environments, Rev. Mod. Phys. **88**, 045006 (2016).

[7] C. O. Reichhardt and C. Reichhardt, Ratchet effects in active matter systems, Annu. Rev. Condens. Matter Phys. **8**, 51 (2017).

[8] L. Angelani, A. Costanzo, and R. Di Leonardo, Active ratchets, Europhys. Lett. **96**, 68002 (2011).

[9] P. Galajda, J. Keymer, P. Chaikin, and R. Austin, A wall of funnels concentrates swimming bacteria, J. Bacteriol. **189**, 8704 (2007).

[10] A. Kaiser, A. Peshkov, A. Sokolov, B. ten Hagen, H. Löwen, and I. S. Aranson, Transport Powered by Bacterial Turbulence, Phys. Rev. Lett. **112**, 158101 (2014).

[11] N. Koumakis, A. Lepore, C. Maggi, and R. Di Leonardo, Targeted delivery of colloids by swimming bacteria, Nat. Commun. **4**, 2588 (2013).

[12] A. Bricard, J.-B. Caussin, N. Desreumaux, O. Dauchot, and D. Bartolo, Emergence of macroscopic directed motion in populations of motile colloids, Nature (London) **503**, 95 (2013).

[13] F. Kümmel, B. ten Hagen, R. Wittkowski, I. Buttinoni, R. Eichhorn, G. Volpe, H. Löwen, and C. Bechinger, Circular Motion of Asymmetric Self-Propelling Particles, Phys. Rev. Lett. **110**, 198302 (2013).

[14] G. Gompper, R. G. Winkler, T. Speck, A. Solon, C. Nardini, F. Peruani, H. Löwen, R. Golestanian, U. B. Kaupp, L. Alvarez, T. Kiørboe, E. Lauga, W. C. K. Poon, A. DeSimone, S. Muiños-Landin, A. Fischer, N. A. Söker, F. Cichos, R. Kapral, P. Gaspard *et al.*, The 2020 motile active matter roadmap, J. Phys.: Condens. Matter **32**, 193001 (2020).

[15] G. De Magistris and D. Marenduzzo, An introduction to the physics of active matter, Physica A **418**, 65 (2015).

[16] H. C. Berg and D. A. Brown, Chemotaxis in *Escherichia coli* analysed by three-dimensional tracking, Nature (London) **239**, 500 (1972).

[17] C. Jones, M. Gomez, R. M. Muoio, A. Vidal, R. A. Mcknight, N. D. Brubaker, and W. W. Ahmed, Stochastic force dynamics of the model microswimmer *chlamydomonasreinhardtii*: Active forces and energetics, Phys. Rev. E **103**, 032403 (2021).

[18] J. R. Howse, R. A. L. Jones, A. J. Ryan, T. Gough, R. Vafabakhsh, and R. Golestanian, Self-Motile Colloidal Particles: From Directed Propulsion to Random Walk, Phys. Rev. Lett. **99**, 048102 (2007).

[19] S. A. Mallory, C. Valeriani, and A. Cacciuto, An active approach to colloidal self-assembly, Annu. Rev. Phys. Chem. **69**, 59 (2018).

[20] C. Scholz, M. Engel, and T. Pöschel, Rotating robots move collectively and self-organize, Nat. Commun. **9**, 1 (2018).

[21] S. Palagi and P. Fischer, Bioinspired microrobots, Nat. Rev. Mater. **3**, 113 (2018).

[22] O. Dauchot and V. Démery, Dynamics of a Self-Propelled Particle in a Harmonic Trap, Phys. Rev. Lett. **122**, 068002 (2019).

[23] A. Cavagna, L. Del Castello, I. Giardina, T. Grigera, A. Jelic, S. Melillo, T. Mora, L. Parisi, E. Silvestri, M. Viale *et al.*, Flocking and turning: A new model for self-organized collective motion, J. Stat. Phys. **158**, 601 (2015).

[24] J. Jhawar, R. G. Morris, U. Amith-Kumar, M. Danny Raj, T. Rogers, H. Rajendran, and V. Guttal, Noise-induced schooling of fish, Nat. Phys. **16**, 488 (2020).

[25] B. ten Hagen, S. van Teeffelen, and H. Lowen, Non-gaussian behaviour of a self-propelled particle on a substrate, Condens. Matter Phys. **12**, 725 (2009).

[26] B. ten Hagen, S. van Teeffelen, and H. Löwen, Brownian motion of a self-propelled particle, J. Phys.: Condens. Matter **23**, 194119 (2011).

[27] K. Malakar, A. Das, A. Kundu, K. V. Kumar, and A. Dhar, Steady state of an active brownian particle in a two-dimensional harmonic trap, Phys. Rev. E **101**, 022610 (2020).

[28] H. Löwen, Inertial effects of self-propelled particles: From active brownian to active langevin motion, J. Chem. Phys. **152**, 040901 (2020).

[29] B. Lehle and J. Peinke, Analyzing a stochastic process driven by ornstein-uhlenbeck noise, Phys. Rev. E **97**, 012113 (2018).

[30] L. L. Bonilla, Active ornstein-uhlenbeck particles, Phys. Rev. E **100**, 022601 (2019).

[31] D. Martin, J. O'Byrne, M. E. Cates, É. Fodor, C. Nardini, J. Tailleur, and F. van Wijland, Statistical mechanics of active ornstein-uhlenbeck particles, Phys. Rev. E **103**, 032607 (2021).

[32] M. E. Cates, Diffusive transport without detailed balance in motile bacteria: Does microbiology need statistical physics? Rep. Prog. Phys. **75**, 042601 (2012).

[33] M. E. Cates and J. Tailleur, When are active brownian particles and run-and-tumble particles equivalent? consequences for motility-induced phase separation, Europhys. Lett. **101**, 20010 (2013).

[34] N. Koumakis, C. Maggi, and R. Di Leonardo, Directed transport of active particles over asymmetric energy barriers, Soft Matter **10**, 5695 (2014).

[35] P. K. Ghosh, V. R. Misko, F. Marchesoni, and F. Nori, Self-Propelled Janus Particles in a Ratchet: Numerical Simulations, Phys. Rev. Lett. **110**, 268301 (2013).

[36] A. Pototsky, A. M. Hahn, and H. Stark, Rectification of self-propelled particles by symmetric barriers, Phys. Rev. E **87**, 042124 (2013).

[37] K. Bisht and R. Marathe, Rectification of twitching bacteria through narrow channels: A numerical simulations study, Phys. Rev. E **101**, 042409 (2020).

[38] B.-Q. Ai and F.-G. Li, Transport of underdamped active particles in ratchet potentials, Soft Matter **13**, 2536 (2017).

[39] G.-h. Xu and B.-q. Ai, Rotation reversal of a ratchet gear powered by active particles, Soft Matter **17**, 7124 (2021).

[40] M. Hatatani, Y. Okamoto, D. Yamamoto, and A. Shioi, Reversed spin of a ratchet motor on a vibrating water bed, Sci. Rep. **12**, 14141 (2022).

[41] F. Q. Potiguar, G. A. Farias, and W. P. Ferreira, Self-propelled particle transport in regular arrays of rigid asymmetric obstacles, Phys. Rev. E **90**, 012307 (2014).

[42] M. B. Wan, C. J. Olson Reichhardt, Z. Nussinov, and C. Reichhardt, Rectification of Swimming Bacteria and Self-Driven Particle Systems by Arrays of Asymmetric Barriers, Phys. Rev. Lett. **101**, 018102 (2008).

[43] M. Mijalkov and G. Volpe, Sorting of chiral microswimmers, Soft Matter **9**, 6376 (2013).

[44] L. Angelani, R. Di Leonardo, and G. Ruocco, Self-Starting Micromotors in a Bacterial Bath, Phys. Rev. Lett. **102**, 048104 (2009).

[45] D. McDermott, C. J. Olson Reichhardt, and C. Reichhardt, Collective ratchet effects and reversals for active matter particles on quasi-one-dimensional asymmetric substrates, Soft Matter **12**, 8606 (2016).

[46] Cs. Sándor, A. Libál, C. Reichhardt, and C. J. Olson Reichhardt, Collective transport for active matter run-and-tumble disk systems on a traveling-wave substrate, Phys. Rev. E **95**, 012607 (2017).

[47] G. Lambert, D. Liao, and R. H. Austin, Collective Escape of Chemotactic Swimmers through Microscopic Ratchets, Phys. Rev. Lett. **104**, 168102 (2010).

[48] J. A. Drocco, C. J. Olson Reichhardt, and C. Reichhardt, Bidirectional sorting of flocking particles in the presence of asymmetric barriers, Phys. Rev. E **85**, 056102 (2012).

[49] Y.-f. He, B.-q. Ai, C.-x. Dai, C. Song, R.-q. Wang, W.-t. Sun, F.-c. Liu, and Y. Feng, Experimental Demonstration of a Dusty Plasma Ratchet Rectification and Its Reversal, Phys. Rev. Lett. **124**, 075001 (2020).

[50] B. Lindner, L. Schimansky-Geier, P. Reimann, P. Hänggi, and M. Nagaoka, Inertia ratchets: A numerical study versus theory, Phys. Rev. E **59**, 1417 (1999).

[51] R. Bartussek, P. Reimann, and P. Hänggi, Precise Numerics versus Theory for Correlation Ratchets, Phys. Rev. Lett. **76**, 1166 (1996).

[52] A. Noushad, S. Shajahan, and M. Sahoo, Velocity auto correlation function of a confined brownian particle, Eur. Phys. J. B **94**, 202 (2021).

[53] M. Muhsin, M. Sahoo, and A. Saha, Orbital magnetism of an active particle in viscoelastic suspension, Phys. Rev. E **104**, 034613 (2021).

[54] M. Muhsin and M. Sahoo, Inertial active ornstein-uhlenbeck particle in the presence of a magnetic field, Phys. Rev. E **106**, 014605 (2022).

[55] J. Tailleur and M. E. Cates, Sedimentation, trapping, and rectification of dilute bacteria, Europhys. Lett. **86**, 60002 (2009).

[56] E. Fodor, C. Nardini, M. E. Cates, J. Tailleur, P. Visco, and F. van Wijland, How Far from Equilibrium Is Active Matter? Phys. Rev. Lett. **117**, 038103 (2016).

[57] D. Mandal, K. Klymko, and M. R. DeWeese, Entropy Production and Fluctuation Theorems for Active Matter, Phys. Rev. Lett. **119**, 258001 (2017).

[58] B.-q. Ai, Directed transport driven by the transverse wall vibration, J. Chem. Phys. **131**, 054111 (2009).

[59] B. Lindner and E. M. Nicola, Diffusion in different models of active brownian motion, Eur. Phys. J.: Spec. Top. **157**, 43 (2008).

[60] H. Risken, *The Fokker-Planck Equation*, 3rd ed., Springer Series in Synergetics (Springer, Berlin, Heidelberg, 1996).

[61] R. F. Fox, I. R. Gatland, R. Roy, and G. Vemuri, Fast, accurate algorithm for numerical simulation of exponentially correlated colored noise, Phys. Rev. A **38**, 5938 (1988).